HHS Public Access

Author manuscript

ACS Appl Nano Mater. Author manuscript; available in PMC 2024 February 26.

Published in final edited form as:

ACS Appl Nano Mater. 2024 January 26; 7(2): 2176–2189. doi:10.1021/acsanm.3c05464.

Doxorubicin-Based Ionic Nanomedicines for Combined Chemo-Phototherapy of Cancer

Mujeebat Bashiru,
Department of Chemistry, University of Arkansas at Little Rock, Little Rock, Arkansas 72204, United States

Samantha Macchi,
Department of Chemistry, University of Arkansas at Little Rock, Little Rock, Arkansas 72204, United States

Mavis Forson,
Department of Chemistry, University of Arkansas at Little Rock, Little Rock, Arkansas 72204, United States

Amna Khan,
Department of Chemistry, University of Arkansas at Fayetteville, Fayetteville, Arkansas 72701, United States

Arisha Ishtiaq,
Department of Chemistry, University of Arkansas at Little Rock, Little Rock, Arkansas 72204, United States

Adeniyi Oyebade,
Department of Chemistry, University of Arkansas at Little Rock, Little Rock, Arkansas 72204, United States

Corresponding Author: **Noureen Siraj** – *Department of Chemistry, University of Arkansas at Little Rock, Little Rock, Arkansas 72204, United States;* nxsiraj@ualr.edu.

Author Contributions

Conceptualization, M.B. and N.S.; methodology, M.B. and N.S.; validation, N.S.; formal analysis, M.B., S.M., M.F., A.K., A.I., A.O., and N.S.; investigation, M.B., M.F., A.K., A.I., A.O., A.J., and N.S.; resources, M.B., N.A., N.H., R.J.G., and N.S.; data curation, M.B.; writing-original draft preparation, M.B.; writing-review and editing, M.B., S.M., M.F., A.K.O., R.J.G., A.J., and N.S., visualization, M.B., N.A., A.K.O., and R.J.G.; supervision, M.B. and N.S.; project administration, M.B.; and N.S.; funding acquisition, N.S. All authors have read and agreed to the published version of the manuscript.

Supporting Information

The Supporting Information is available free of charge at https://pubs.acs.org/doi/10.1021/acsanm.3c05464.
ESI-MS, NMR spectra, ζ-potential, melting point of synthesized ionic materials; time-dependent DLS plots of [DOX][IR820] INMs in water; normalized absorbance of parent NIR dyes and three chemo-PTT combination drugs in water; fluorescence spectra of DOX and chemo-PTT combination IMs and INMs in ethanol and water, respectively; absorbance of INMs and parent dyes in various media; normalized fluorescence emission spectra of DOX (donor) and absorption spectra of acceptor (NIR dyes) in water and in ethanol; FRET efficiency equation,; table showing the FRET efficiency for all INMs and IMs in the presence of DOX (donor); fluorescence quantum yield and photophysical rate constants; fluorescence quantum yield, radiative rate, and nonradiative rate of all IMs in ethanol excited at 710 nm wavelength; fluorescence quantum yield of INMs and IMs in water and ethanol excited at 480 nm wavelength; photostability results of INM and IM in water and ethanol; PTT efficiency curve for all drugs in pure water and PBS; photodegradation of DPBF upon increasing the irradiation time in the presence of [DOX][ICG] in water; SOQY results for IMs and INMs in ethanol and water; time-dependent cellular uptake results of INMs on MCF-7 cells; cell viability results for NIR dyes and doxorubicin-based drugs in the dark and light; and YO-PRO/propidium iodide staining results for MCF-7 cells treated with [DOX][IR783] INMs and DOX after 6 h drug incubation (PDF)

Complete contact information is available at: https://pubs.acs.org/10.1021/acsanm.3c05464

The authors declare no competing financial interest.

Amanda Jalihal,
Department of Chemistry, University of Arkansas at Little Rock, Little Rock, Arkansas 72204, United States

Nawab Ali,
Department of Biology, University of Arkansas at Little Rock, Little Rock, Arkansas 72204, United States

Robert J. Griffin,
Department of Radiation Oncology, Arkansas Nanomedicine Center, Winthrop P. Rockefeller Cancer Institute, University of Arkansas for Medical Sciences, Little Rock, Arkansas 72205, United States

Adegboyega K. Oyelere,
School of Chemistry and Biochemistry, Parker H. Petit Institute for Bioengineering and Bioscience, Georgia Institute of Technology, Atlanta, Georgia 30332, United States

Nasrin Hooshmand,
Laser Dynamics Laboratory, School of Chemistry and Biochemistry, Georgia Institute of Technology, Atlanta, Georgia 30332, United States

Noureen Siraj
Department of Chemistry, University of Arkansas at Little Rock, Little Rock, Arkansas 72204, United States

Abstract

Synergistic combination therapy approach offers lots of options for delivery of materials with anticancer properties, which is a very promising strategy to treat a variety of malignant lesions with enhanced therapeutic efficacy. The current study involves a detailed investigation of combination ionic nanomedicines where a chemotherapeutic drug is coupled with a photothermal agent to attain dual mechanisms (chemotherapy (chemo) and photothermal therapy (PTT)) to improve the drug's efficacy. An FDA-approved Doxorubicin hydrochloride (DOX·HCl) is electrostatically attached with a near-infrared cyanine dye (ICG, IR783, and IR820), which serves as a PTT drug using ionic liquid chemistry to develop three ionic material (IM)-based chemo-PTT drugs. Carrier-free ionic nanomedicines (INMs) are derived from ionic materials (IMs). The photophysical properties of the developed combination IMs and their INMs were studied in depth. The phototherapeutic efficiency of the combination drugs was evaluated by measuring the photothermal conversion efficiency and singlet-oxygen quantum yield. The improved photophysical properties of the combination nanomedicines in comparison to their parent compounds significantly enhanced INMs' photothermal efficiency. Cellular uptake, dark and light toxicity studies, and cell death mechanisms of the chemo-PTT nanoparticles were also studied *in vitro*. The combination INMs exhibited enhanced cytotoxicity compared to their respective parent compounds. Moreover, the apoptosis cell death mechanism was almost doubled for combination nanomedicine than the free DOX, which is attributed to enhanced cellular uptake. Examination of the combination index and improved *in vitro* cytotoxicity results revealed a great synergy between chemo and PTT drugs in the developed combination nanomedicines.

Graphical Abstract

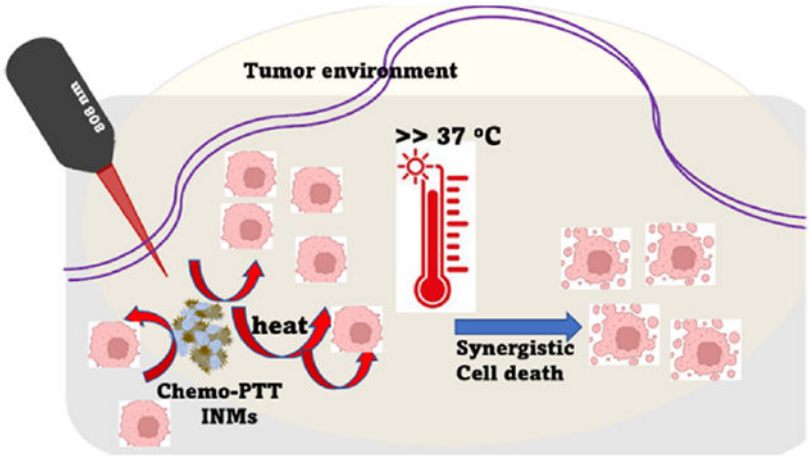

Keywords

combination therapy; ionic nanomaterial; doxorubicin; photothermal therapy; cytotoxicity; cell death mechanism

INTRODUCTION

Despite improvements in prevention, early detection, and available treatment options, the latest annual reports from the National Cancer Institutes for cancer statistics revealed an increasing trend in cancer incidence and mortality rate.[1–4] Numerous cancer types, including breast cancer, melanoma, kidney, and pancreatic cancer, have been treated using conventional methods such as surgery, chemotherapy, radiation therapy, and immunotherapy.[5] However, some of these strategies are limited due to invasiveness, side effects imposed from lack of specificity, selectivity, and multidrug resistance (MDR).[6–8] Recently, non-invasive NIR-mediated phototherapy techniques such as photothermal and photodynamic therapies (PTT and PDT) have been explored for cancer treatment.[9] PTT involves the use of photothermal agents (PTAs) to produce heat upon absorption of light, resulting in hyperthermia that leads to cancerous cell death.[9–11] The discovery that the heat created by PTAs also lowers interstitial fluid pressure and enhances blood circulation, in addition to direct killing of tumor cells, makes PTT a promising treatment option.12

Cyanine dyes like indocyanine green (ICG), an FDA-approved drug, are studied for cancer treatment, imaging diagnosis, and drug delivery applications.[13–19] The use of other NIR cyanine dyes, such as IR783 and IR820, is also gaining significant attention for cancer applications.[19,20] Normally, dyes that absorb the visible wavelength region of the electromagnetic radiation spectrum are used for treatment of skin infections. However, PTAs that absorb light in the therapeutic NIR window (above 780 nm) exhibit deeper penetration depth in body tissues. Thus, it is favorable to treat deeply seated malignancies. Despite their selectivity, ICG exhibits concentration-dependent aggregation, light sensitivity, and a short blood half-life of 2–4 min in aqueous environments, hindering its use in

medicine.[13,17] Similarly, the hydrophilic properties and shelf life of IR783 and IR820 are also disadvantages for direct *in vitro* and *in vivo* use. These NIR dyes are poorly absorbed by the body due to their hydrophilic nature, which causes rapid excretion.[21] Therefore, these soluble PTAs have been modified mostly using inorganic and organic nanocarriers.[22,23] However, some of these nanocarriers are imposing unwanted processes such as absorption, distribution, metabolism, and excretion (ADME profile) of the drug when used for biological purposes.[24] Thus, there is a need for new, simple, and economical strategies to optimize the performance of NIR dyes. Among others, combination therapy and carrier-free nanomedicines based on NIR dyes are promising approaches to developing ideal drugs.

Combination therapy involves combining more than one therapeutic mechanism in a drug to treat tumors effectively. Moreover, combination therapy can address several drawbacks associated with single therapy such as MDR, solubility, and dosage-related problems. Combination medicines can perform better than single drugs owing to the powerful synergistic effect of multimodal therapeutics. Studies have revealed that PTT and chemotherapy complement each other by enhancing drug performance in the combination form compared to individual parent drugs.[21,25,26] Most combination therapeutics involve active agents developed via costly, multiple-step, and complicated organic synthesis commonly known for a very low product yield.[21,25,27–29] Thus, it is of utmost importance to implement new economical and simple synthesis strategies for the development of combination drugs.

Recently, nanotechnology involving the use of nanocarriers and nanovehicles has served as a promising approach to cancer treatment. Tumor cells have poorly aligned and leaky vessels, thus making the accumulation of nanosized drugs have better penetration and retention capabilities within the tumor.[30] Additionally, the use of nanoparticles for drug delivery offers benefits such as targeting certain cells and safeguarding sensitive therapeutics against premature deterioration, all of which can help mitigate negative effects.[31] Unfortunately, most studied nanomaterials are metal-based, such as gold, and iron oxide nanoparticles having significant limitations in the biological system, owing to their non-biodegradable and non-biocompatible features. These nanomaterials require further appropriate surface functionalization and special synthetic methods in order to be used for clinical application.[32–34] Thus, carrier-free nanodrugs composed of soft organic materials that are highly biocompatible and biodegradable are an excellent choice for cancer treatment at present.

Herein, three new chemo-PTT combination ionic nanomedicines (INMs) are designed using an FDA-approved chemo drug (Doxorubicin hydrochloride, i.e., DOX·HCl) and an NIR dye (ICG, IR783, and IR820) by employing ionic liquid (IL) chemistry. The simple and economical synthesis of ionic materials (IMs) with distinct properties are useful for biological applications.[35] Their excellent thermal stability, high photostability, and most importantly ease of tunability are a few of these qualities that make the IL-approach simple to use in the synthesis of chemo-PTT combination IMs.[6,36] The selected FDA approved chemo (DOX) and photothermal therapeutic agents in the INMs form were used for the treatment of MCF-7 cancer cells. DOX is known for its DNA-binding properties,

topoisomerase II inhibition, and production of free radicals capable of causing programmed cell death (apoptosis).[7,37] It is anticipated that the use of combination therapy will significantly minimize the dose of the chemo and PTT drugs, thereby addressing multidrug resistance (MDR), minimizing side effects to normal cells, and producing a synergistic effect of both the chemo and PTT drug with improved therapeutic efficacy. In addition, the heat produced by the PTT drug upon laser irradiation can also contribute to better drug uptake by the cells, thereby boosting the therapeutic potency of the chemo-PTT combination nanodrug.[38] The newly synthesized distinct chemo-PTT INMs were examined for their physicochemical properties, photophysical characteristics, light-to-heat efficiency, singlet oxygen quantum yield, cellular uptake, *in vitro* cytotoxicity, and apoptosis mechanism to provide insights regarding their potential as combination anticancer nanomedicines. As far as we know, this is the first report employing IL chemistry for developing combination nanomedicine using an FDA-approved drug (DOX·HCl).

EXPERIMENTAL SECTION

Chemicals.

Doxorubicin hydrochloride (DOX·HCl), 2-[2-[2-Chloro-3-[2-[1,3-dihydro-3,3-dimethyl-1-(4-sulfobutyl)-2H-indol-2-ylidene]-ethylidene]-1-cyclohexene-1-yl]-ethenyl]-3,3-dimethyl-1-(4-sulfobutyl)-3H-indolium hydroxide inner salt, sodium salt (NaIR783, Lot # BCBZ9950), 2-[2-[2-chloro-3-[[1,3-dihydro-1,1-dimethyl-3-(4-sulfobutyl)-2H-benzo[*e*]indol-2-ylidene]-ethylidene]-1-cyclohexen-1-yl]-ethenyl]-1,1-dimethyl-3-(4-sulfobutyl)-1H-benzo[*e*]indolium hydroxide inner salt, sodium salt (NaIR820, Lot # SHBM1333), and 1,3-diphenylisobenzofuran (DPBF, Lot # STBD0599 V) were purchased from Sigma-Aldrich (St. Louis, MO). Indocyanine green (NaICG, lot no. KV5YO-LG) was purchased from Tokyo Chemical Industry (Tokyo, Japan). The pure lab ultrapure water purification system was used to provide triply deionized water (18.2 M cm; ELGA, Woodridge, IL). ACS-grade dichloromethane (DCM) and ethanol were obtained from Thermo Fischer Scientific (Waltham, MA). The 808 nm laser was purchased from Opto Engine LLC (Midvale, UT). MCF-7 breast cancerous cells were obtained from the American Type Culture Collection (ATCC, Manassas, VA). Penicillin streptomycin and Trypsin-EDTA (0.25%) were both purchased from Caisson Lab (Smithfield, UT). MTT (3-(4,5-dimethylthiazol-2-yl)-2,5-diphenyltetrazolium bromide), 4′,6-diamidino-2-phenylindole (DAPI), Cell media (Dulbecco's modified Eagle's medium (DMEM)), phosphate-buffered saline (PBS) pH 7.4, and dimethyl sulfoxide (DMSO) were all purchased from Sigma-Aldrich, (St. Louis, MO). Fetal bovine serum (FBS) was obtained from Atlanta Biologicals (Lawrenceville, GA). YO-PRO (lot no. 1597071) was purchased from Thermo Fisher Scientific, and propidium iodide PI (lot no. 21P0211) was obtained from Biotium.

Characterization of Doxorubicin-Based Chemo Combination Drugs.

Electrospray ionization mass spectrometry (ESI-MS) was used to characterize the chemo-PTT combination IMs utilizing a Bruker (Billerica, MA) Ultraflex 9.4T in methanol solvent. This technique was used to confirm the presence of both cation and anion in all three combination drugs, with peaks corresponding to the mass-to-charge ratio in the positive

and negative ion modes, as shown in Figure S1. These chemo-PTT IMs were further characterized with a JEOL 400 MHz nuclear magnetic resonance (NMR) instrument, using deuterated DMSO solvent as shown in Figure S2.

Characterization of INMs.

The dynamic light scattering (DLS) method was utilized to estimate the hydrodynamic diameter as well as the polydispersity index of the INMs in DI water using a Zetasizer pro red Malvern Instrument (Malvern Panalytical Limited, Worcestershire, U.K.). Additionally, the size of the INMs was verified using transmission electron microscopy (TEM) with a JEOL FEI Tecnai F20 200 keV microscope.

Photophysical Characterization.

Absorption spectra of the parent compounds, the synthesized IMs, and the INMs were recorded using a UV–visible spectrophotometer (Agilent Cary 5000, Santa Clara, CA), while their fluorescence emission spectra were recorded using a fluorometer (Horiba FluoroMax, Kyoto, Japan). For absorbance measurement, a polished two-sided quartz cuvette with a 10 mm path length (Starna cells) was used against an identical control cell filled with the sample's solvent. Fluorescence measurements were performed using a four-sided Starna quartz cuvette having a 1 cm path length. An identical slit width, 0.1 s integration time, and right-angle geometry were used for all samples' measurements. Fluorescence quantum yield measurement was performed for all NIR-containing compounds using a relative method by employing NaICG as the standard with a reported fluorescence quantum yield value of 0.14 in ethanol.[39]

Fluorescence Lifetime Measurement.

A Horiba fluorometer featuring a Delta Hub controller and time-correlated single photon counting (TCSPC) was used to measure the fluorescence lifetime for the combination of IMs in ethanol. A 455 nm wavelength NanoLED served as the excitation source for measurement. Using exponential fitting of the raw data, the lifetime data were examined using DAS6 software.

Light-to-Heat Conversion Efficiency.

Investigation of the photothermal effect of any drug requires subjecting the PTA to laser irradiation and monitoring the change in the temperature over time. The heat efficiency of the NIR parent dyes and chemo-PTT combination INMs was investigated to determine the drug's PTT potency. To examine the PTT effects of the various NIR parent compounds, the drugs were prepared in different solvents such as pure water, PBS, and cell media containing FBS. A similar concentration of each INM was prepared in various media via the reprecipitation method as previously stated and was left to stabilize for 20 min prior to the experiment. In a typical experiment, 1 mL of 50 μM solution of the various samples (NIR parent dyes and INMs) was subjected to a 5 min laser treatment (808 nm, 1 W cm^{-2}). The temperature of the entire solution was measured using a thermocouple probe every 30 s. The sample was irradiated with 808 nm laser light for the first 5 min, and for the next 5 min, the sample's cooling temperature was recorded after the laser was turned off.

Singlet Oxygen Quantum Yield (SOQY).

Photosensitizer (PS) capable of absorbing light upon irradiation can get promoted to the excited triplet state from the excited singlet state via a nonradiative pathway known as intersystem crossing. At the excited triplet state, the PS reacts with molecular oxygen present to produce reactive oxygen species (ROS).[40] Literature has shown that NIR-absorbing dyes such as NaICG, NaIR783, and NaIR820 can produce ROS upon absorption of light and are dependent on the media. The SOQY efficiencies of NIR dyes are fairly low in water (around 0.8%)[41,42] but very high (around 20%) in other media.[43,44]

To ascertain the PDT effect by the NIR dyes in comparison to the newly synthesized combination drugs, an SOQY experiment was conducted. The experiment was performed using parent dyes, combination IMs, and INMs. It is very important to understand the role of the chemotherapeutic cation (DOX) on the ROS production of NIR dyes in the combination of IMs and nanomedicines. Therefore, a parent NIR dye solution, combination IM, or INMs was mixed independently with DPBF probe solution in ethanol for the SOQY experiment. In a typical experiment, DPBF and the parent NIR drug were dissolved in ethanol, separately. A concentration of 5 μM drug in 100 μM DPBF was achieved by mixing an equal volume of DPBF and a drug solution. By measuring the decrease in absorbance at 411 nm after exposing the solution mixture to 808 nm laser (1 W cm^{-2}) for 15 s at a time for a total of 60 s, the rate of ROS formation was calculated. A UV/vis spectrophotometer was used to track the decrease in absorbance of DPBF at 411 nm after each 15 s exposure. The parent NIR dyes and the combination drug's ROS quantum yields in ethanol were calculated using NaIR820 as a reference.[26]

For the SOQY experiment involving the INMs, only IMs and DPBF were prepared in DMSO separately and then nanoparticles were prepared via a reprecipitation method. To prepare the INMs, we initially prepared a stock solution of IMs or DPBF in DMSO. INMs were prepared by adding an aliquot of IM dropwise to the vial containing water in an active sonication bath left to sonicate for 5 min and proceeded with a 20 min stabilization prior to any measurement. The parent NIR soluble dyes were prepared directly in water. The final concentration of the resultant solution (parent NIR dyes or INMs) used was 10 μM drug in 25 μM DPBF. A similar irradiation protocol was followed, and the formation of singlet oxygen was detected by measuring the decrease in DPBF absorbance at 411 nm. This was quantified using eq 1.

A control experiment in which a solution of DPBF in ethanol was irradiated under identical conditions was designed to verify that the decrease in absorbance at 411 nm is caused by the drug.

$$\phi\,\Delta\,(x) = \phi\,\Delta\,(\mathrm{std}) \times \frac{S_x}{S_{\mathrm{std}}} \tag{1}$$

where $\phi\,\Delta\,(\mathrm{std})$ denotes the ROS quantum yield of the standard.

S_x and S_{std} are the slopes obtained from the absorbance vs time graph showing the decrease in DPBF absorbance at 411 nm for unknown and standard samples, respectively. By comparing the absorbance decrease of the probe in the presence of combination INMs, NaIR783 was employed as the standard to compute the SOQY according to eq 1. The ROS quantum yield of chemo-PTT INMs and IMs was calculated using references with reported literature values of 0.7% in water and 7.7% in ethanol for NaIR783 and NaIR820, respectively.[6,45]

Photostability Measurements.

Photostability of the various free NIR dyes and chemo-PTT combination drug was investigated by kinetically measuring the fluorescence emission intensity over a 30 min period at intervals of 0.1 s. A quartz cuvette with a four-sided polished window and a 1 cm path length was used for the measurements. Briefly, a 2 μM solution of the parent compound and the chemo-PTT combination drug was prepared from ethanol stock, and the photostability measurement was performed using the absorbance wavelength maxima as the excitation wavelength and recording the fluorescence emission at respective fluorescence emission maxima wavelength of compounds. The excitation and emission slit widths were both adjusted to 14/14 nm.

Cellular Uptake.

The detailed characterization of the drug is performed *in vitro* to investigate its therapeutic potential. For the test, only MCF-7 cells were used for all *in vitro* experiments. The potential of these drugs in other cell lines as well as in normal cell lines will be presented in another paper. Since combination drugs are being used in a nanoparticle form as compared to their soluble parent chemo and PTT drugs, it may impact the cellular uptake and consequently affect the cytotoxicity. Therefore, cellular uptake tests were carried out to ascertain the concentration of drugs internalized by MCF-7 cells over a specific period. In a typical experiment, 6×10^5 cells were seeded and left to incubate for 24 h in a six-well plate. A 20 μM concentration of parent NIR dyes, soluble chemo drugs, or INMs was introduced to each well with a total volume of 3 mL in each well and incubated for 6 h. Uninternalized drugs were eliminated after the stipulated period, and cells were carefully washed repeatedly thrice with PBS. Cells were further broken up by addition of 3 mL of DMSO, allowing the internalized drug to be quantified by a UV–vis absorbance spectrophotometer.

Cell Culture/Cell Viability Studies.

For *in vitro* experiments, a monolayer of MCF-7 cell lines was maintained in complete media at 37 °C and 5% CO_2. MCF-7 cells were grown in DMEM supplemented with FBS (10% v/v) and an antibiotic solution containing penicillin/streptomycin (500 units/mL). When cells reached the desired confluency, they were trypsinized to subculture, and the detached cells were counted using a hemocytometer after being stained with the trypan blue exclusion dye. For a 24 h dark cytotoxicity experiment, 10^4 cells per well were plated in 96-well plates and incubated at 37 °C and 5% CO_2. After that, cells were exposed to various INM concentrations for 24 h. Different concentrations of INMs were prepared by reprecipitating the stock solution in DMEM media under sonication while maintaining a sterile environment. To prevent any cellular toxicity from DMSO, the amount of DMSO

used was limited to a maximum of 0.5%. For each experiment, complete media controls and DMSO controls were taken into consideration. PBS was used to wash the cells before the treatment. MTT assay was used to determine cell viability. The optical density of MTT-formazan at 570 nm was measured by using a microplate reader (Biotek Synergy H1, Winooski, VT). For *in vitro* experiments, each experiment was carried out in triplicate and repeated thrice. Except as otherwise stated, all data with error bars are provided as mean ± standard deviation (SD). The two-tailed Student's "*t*" test was used to evaluate the significant difference in the mean values. Values that differ significantly are shown by the symbols $*p < 0.05$, $**p < 0.01$, and $***p < 0.005$.

Light cytotoxicity experiments were performed to ascertain the PTT efficiency of the parent NIR drugs as well as the PTA present with DOX in the combination INMs. Cells were treated in a similar manner as that described above. In a typical experiment, 10^4 cells were seeded in a 96-well plate in alternate wells and incubated for 24 h. Cells were further treated with INMs or parent dyes and incubated for 6 h to minimize the cytotoxic effect from DOX while trying to elucidate mostly the PTT effect. After 6 h of drug incubation, the media containing drug was aspirated, and the cells were washed twice with PBS to remove the external uninternalized drugs. Cell media was replaced in each well, and each well plate was exposed for 5 min to a near-infrared laser (808 nm, 1 W cm^{-2}). After 24 h incubation, the MTT assay was used to investigate the cytotoxicity of the NIR dyes. A control experiment without any PTA containing drug was subjected to light and conducted under similar conditions.

Cell Death Mechanism.

Cell death mechanism was investigated using a caspase assay and flow cytometry.

For caspase 3/7 staining, cells were plated at a density of 2×10^5 per well in a 24-well plate with preintroduced coverslips and were incubated for 24 h. Cells were treated with 5 μM INMs prepared in cell media after being washed with PBS and then followed by incubation for 6 h. After the stipulated time, the uninternalized drugs were aspirated and the cells were treated with 5 μM caspase 3/7 assay for 60 min. Fixation of the cells was done with 4% paraformaldehyde for 15 min. Cells were permeabilized for 30 min using a blocking solution (0.3 M glycine, 10% BSA, and 1% saponin in PBS). Cells were further washed with PBS prior to the addition of DAPI (nuclear stain) at 300 nM concentration. Cells were washed with PBS before mounting on the glass slide and imaged using the laser scanning confocal microscope (Zeiss, LSM 800).[46]

For flow cytometry using PI (propidium iodide)/YO-PRO staining, cells were plated at approximately 1×10^6 cells in a six-well plate and incubated overnight. Cells were washed with PBS and incubated with 5 μM INMs for 6 or 48 h. After drug treatment, both floating and adherent cells were harvested by addition of 0.5 mL of trypsin and monitored closely for complete detachment of cells under the microscope. Trypsin was neutralized with 1 mL of serum containing media, and the cell mixture was transferred into a centrifuge tube and proceeded with spinning at 1100 rpm for 5 min. The cell pellet was washed with cold PBS and recentrifuged again for 5 min. Cells were resuspended in a 0.25–0.5 mL PBS in flow cytometry tubes, followed by addition of 1 μL of PI and YO-PRO solutions to the cell

mixture according to the manufacturer's protocol. The tubes were all placed in an ice bath and proceeded for flow cytometry data acquisition.[47]

Statistics.

The two-tailed Student's *t* test was used for statistical analysis. Statistical significance was defined as *p*-values of $*p < 0.05$, $**p < 0.01$, and $***p < 0.005$. The mean ± SD is used to express the results, which are representative of at least three studies.

RESULTS AND DISCUSSION

Synthesis and Characterization of Doxorubicin-Based Chemo Combination Drugs (IMs).

Three chemo-PTT combination drugs were synthesized from two ionic parent compounds using a simplistic, rapid, economical, onestep ion-exchange method, as shown in Figure 1a. For synthesis of [DOX][ICG], equivalent mole ratios of DOX and NaICG were separately dissolved in water. Aqueous solutions of both DOX and NaICG were combined, and the precipitate of the [DOX][ICG] combination IMs was observed immediately. To make sure the ion-exchange reaction was complete, the mixture was agitated continuously for 24 h. The resultant mixture was centrifuged at 3800 rpm for 5 min, and the supernatant was removed to recover the precipitate of IMs. The precipitate was washed three times with water to remove the byproduct (NaCl). The resultant drug [DOX][ICG] was lyophilized to remove moisture impurities from IMs before use for further studies. Since NaIR783 and NaIR820 are also hydrophilic, a similar protocol was followed to synthesize the [DOX][IR783] and [DOX][IR820] chemo-PTT combination drugs, respectively, as shown in Figures S3 and S4.

All IMs were characterized in detail to investigate the presence of cations and anions in the combination drugs as well as the purity of the compound. Synthesized IMs, [DOX][ICG], [DOX][IR820], and [DOX][IR783] were characterized using ESI-MS. The presence of both the cation and anion was verified by the mass-to-charge ratio peaks in the positive and negative ion modes. Mass spectra data for all compounds are shown in Figure S1. NMR spectroscopy was also used to characterize the IMs. NMR spectra and results are presented in Figure S2.

After the purity of the materials was confirmed, the compounds were further characterized to investigate their physicochemical properties. The melting points of [DOX][ICG], [DOX][IR820], and [DOX][IR783] INMs were 230, 233, and 212 °C, respectively. Table S1 shows the melting point range for all of the compounds compared with their parent NIR dyes. The melting points of all combination drugs are under 250 °C.

Synthesis and Characterization of INMs.

INMs were prepared by a reprecipitation method in water or cell media from the IMs as shown in Figure 1b. These are carrier-free nanoparticles that were prepared in pure water/cell media under sonication. In a nutshell, 1 mM concentration of the chemo-PTT combination IMs was initially prepared in ethanol or dimethyl sulfoxide (DMSO). To a scintillation vial containing deionized water or cell media in an active sonication bath,

a small amount of the stock solution was introduced dropwise. The sample (INMs) was sonicated for 5 min and stabilized for 20 min before performing any experiments. The shape and size of nanoparticles were characterized in detail.

Physical properties of INMs were investigated in detail by using different techniques. The shape and size of the INMs were determined by using transmission electron microscopy (TEM). The INMs were found to be spherical in shape as shown in Figure 2a–c. The observed sizes for [DOX][ICG], [DOX][IR783], and [DOX][IR820] were found to be 135 ± 12.5, 174 ± 22.5, and 105 ± 15.9 nm respectively. NPs with diameters between 10 and 200 nm have been reported to actively target malignant tissues due to the EPR effects.[26] Zeta (ζ)-potential measurements were performed using Zetasizer pro red Malvern equipment. The ζ-potential results reported in Table S2 showed that all nanoparticles exhibited a very low negative surface charge, which suggests that the NIR dyes mainly residing at the surface of the nanomaterials. All three INMs also exhibit a polydispersity index less than 0.30 (Table S2), which indicates a homogeneous population of the nanodrug.[48,49] [DOX][ICG] exhibited the lowest PDI, whereas [DOX][IR783] depicted the highest PDI, which is attributed to its lowest ζ-potential value. Dynamic light scattering (DLS) experiments were performed at various intervals to test the stability of the nanoparticles. Examination of data revealed that the [DOX][IR820] INMS were stable for 24 h as shown in Figure S5.

Photophysical Characterization.

The photothermal efficiency of a PTA mainly relies on its photophysical properties. The photophysical characteristics of parent NIR dye compounds and combination IMs and INMs were investigated in water and ethanol as shown in Figures 3, S6, and S7. The absorption maxima wavelength, molar absorptivity, fluorescence emission, and quantum yield were determined since all of these key photophysical parameters can influence the phototherapeutic activities such as reactive oxygen species (ROS) quantum yield and the light-to-heat conversion efficiency of the PTA in the presence of the DOX cation in the combination IMs and INMs. Hence, the changes in the absorption and fluorescence spectra of the combination drug in water and ethanol were investigated and compared with their respective parent compounds to determine the effect of the counterion.

Absorption spectra results confirmed the presence of both cations (DOX) and anions (NIR dye) in the IMs and INMs. Examination of absorption spectra of ICG compounds revealed that the ICG anion absorption peak exhibited significant broadness when NaICG were converted into combination INMs. In water, both NaICG free dye and [DOX][ICG] INM displayed a similar absorbance peak at 777 nm with a shoulder peak around 720 nm (Figure S6a). However, a slight bathochromic shift occurs for both compounds in ethanol in comparison to water from 777 to 789 nm as shown in Figures S6a and S7a. However, no significant change in the shoulder peak (around 720 nm) was observed for both NaICG and [DOX][ICG] in ethanol.

NaIR820 free dye and its INM, [DOX][IR820], showed two distinct absorbance peaks in water for the IR820 anion (Figures 3 and S6b). Absorbance peaks for NaIR820 were observed at 690 and 813 nm. A bathochromic shift (red shift) was observed in the first peak from 690 to 733 nm (broad), while the peak at 813 nm remained unchanged upon conversion

of NaIR820 into [DOX][IR820] INMs (Figure S6b). Moreover, a very broad absorption peak for IR820 anions was observed in INMs that exhibited significant absorption at a longer wavelength, which is highly desirable due to the deeper penetration of longer wavelength radiation for the treatment of deeply seated tumors. In addition, both NaIR820 and [DOX][IR820] IM in ethanol depicted an absorbance maximum at 830 nm as well as a shoulder peak at 750 nm for the IR820 anion (Figure S7b), which is supported by the literature.[26]

The absorption spectra of the other compounds based on IR783 were also recorded to determine any significant changes in the photophysical properties. The peak shape for IR783 anions did not change significantly when converted from NaIR783 to [DOX][IR783] INMs. For parent compounds NaIR783 and [DOX][IR783] INM in water, both showed an absorbance peak maximum of 774 nm with a shoulder peak at 720 nm for the IR783 anion (Figure S6c). A slight red shift was observed for both compounds in ethanol with an absorbance maximum of 787 nm (Figure S7c) for the IR783 anion. No significant changes in the DOX peak were observed.

As anticipated, a higher molar absorptivity value was observed for the soluble combination IMs than in the nanoparticle form (INMs) except for ICG as reported in Table S3. In contrast, only NaICG shows a greater molar absorptivity value in water than in ethanol. Thus, the absorption characteristics of a photosensitizer depend on the countercation. Herein, the DOX countercation enhanced the absorptivity characteristics of the NIR dyes.

The absorbance of the samples was also recorded in PBS and cell media to mimic the *in vitro* environment. Absorption spectra recorded in cell media and PBS are presented in Figure S8. Both ICG and IR783-based compounds depicted similar peaks. However, significant changes in the peak maxima were observed for IR820-based compounds as shown in Figure S8.

The detailed study of absorption spectra revealed some substantial alterations in the dye's photophysical characteristics. To investigate any changes in the fluorescence emission spectra of the compound, we performed fluorescence measurements. The fluorescence spectra of the IMs (Figure S9a–d) and INMs as compared with the parent drugs are shown in Figures S9e and 3b. When the INMs were excited at the absorbance peak maxima of DOX (480 nm), a similar shape of the fluorescence emission spectrum was observed for the DOX cation with a wavelength maximum at 595 nm along with two shoulder peaks at 555 and 639 nm in all three combination nanomedicines (Figure S9e). Interestingly, the fluorescence emission intensity for the DOX cation in each combination INM decreased significantly as compared to the parent DOX compound. The decrease in fluorescence intensity of [DOX][IR820] and [DOX][ICG] is very similar, while a significant decrease in fluorescence intensity was observed in the [DOX][IR783] INM. This decrease in fluorescence intensity signal for the DOX in all three INMs possibly signifies the existence of the FRET mechanism since there is an overlap between DOX fluorescence emission spectra and NIR dye absorption spectra.

Fluorescence emission spectra for all chemo-PTT materials were also recorded at the excitation wavelength of the NIR dye. The fluorescence emission intensity slightly increased

in all IMs as compared to their respective parent NIR compound in ethanol except for [DOX][IR783] as shown in Figure S9d. However, significant decrease were observed in fluorescence emission intensities of NIR dyes for [DOX][ICG] and [DOX][IR783] in the nanoparticle form in comparison to their parent NIR dyes at 710 nm excitation wavelength, as shown in Figure 3b. This suggests substantial changes in the photophysical properties of the chemo-PTT combination drug when converted from IMs to nanomedicines. The significant decrease in the fluorescence emission intensity of the two INMs suggests an increase in the nonradiative vibrational relaxation process. However, a slight increase in fluorescence intensity was observed for [DOX][IR820] INMs. To better understand these changes in the photophysical properties, the FRET parameters and photophysical rates (radiative and nonradiative rates) were calculated.

To verify the FRET possibility in the newly developed chemo-PTT IMs and INMs, FRET calculations were performed. FRET is a nonradiative energy transfer from a donor molecule to an acceptor molecule that is within 10 nm distance of each other. In this case, DOX represents the donor, while the PTAs are the acceptor molecule. Spectral overlap of donor fluorescence emission and acceptor absorption spectra are depicted in Figure S10 for all INMs and IMs in water and ethanol, respectively. FRET efficiency and other FRET parameters were calculated using eqs S1–S3, and results are shown in Tables S4 and S5. Our group was the first to report the existence of the FRET mechanism in IMs.[50] The FRET results revealed that the newly developed INMs and IMs exhibited FRET efficiency greater than 45%. Moreover, the FRET efficiency is significantly higher in INMs as compared to IMs.

Fluorescence Quantum Yield (FLQY) and Photophysical Rate Constants.

The detailed study of absorption and fluorescence emission suggested tremendous changes in the electronic states of the compounds. Fluorescence quantum yields (FLQY) for parent drugs, IMs, and INMs were all quantified using a relative technique (eq S4). FLQY was calculated at both 480 and 710 nm excitation wavelengths for DOX and the NIR dyes, respectively. Furthermore, radiative and nonradiative rates were calculated using eqs S5 and S6. FLQY values for all INMs and IMs in water and ethanol, recorded at 710 nm excitation wavelength, are listed in Tables 1 and S6, respectively.

FLQY of IMs increased in comparison to the parent NIR dye in ethanol at 710 nm excitation wavelength except for [DOX][IR783] IMs as shown in Table S6. However, the combination drugs in the nanoparticle form showed a decrease in FLQY as compared to the parent NIR dyes in water, as shown in Table 1. The decrease in the FLQY of INMs was likely due to the existence of another dominating non-radiative relaxation pathway (k_{nonrad}). This is evident from the quantitative results that k_{nonrad} obtained for the INMs is greater than their radiative rate (k_{rad}). The higher k_{nonrad} of INMs depicted that the excited-state compound prefers to relax to the ground state via internal conversion or the intersystem crossing route. Detailed examination of these results demonstrated that INMs are promising nanomedicines for phototherapies, which exhibited low FLQY owing to an increased non-radiative process necessary for heat generation as well as for ROS generation. Intriguingly, k_{nonrad} for all INMs was significantly improved compared to their respective parent NIR dyes. To further

investigate the potential of INMs, the fluorescence lifetime and photostability experiments are designed.

Fluorescence Lifetime.

The fluorescence lifetime of the chemo-PTT IMs was also investigated in ethanol, and the data were fitted bi-or tri-exponentially, with χ^2 values close to unity as shown in Table S8. Fluorescence lifetime fitting correlates well with the previously reported mean fluorescence lifetime of DOX in ethanol.[51,52] Interestingly, DOX has been found to exhibit an excitation-dependent fluorescence behavior in different solvents, which could consequently affect the DOX fluorescence lifetime.[52] However, fluorescence lifetime results for IMs in ethanol excited at 455 nm revealed mainly two states, τ_1 and τ_2 (shorter and longer lifetime components), contributing to the fluorescence emission for parent DOX and [DOX][IR820] IM only. For both [DOX][IR783] and [DOX][ICG] IMs, a third lifetime component with a longer lifetime (τ_3) with low abundance (a_3) was observed. Overall quantification of the mean lifetimes for all chemo-PTT IMs in ethanol revealed a shorter-lived excited singlet state for the modified [DOX][IR820] and [DOX][ICG] IMs compared to the parent-free DOX. Only the [DOx][IR783] IM exhibited a longer fluorescence lifetime.

Photostability.

Photostability is one of the most important characteristics of a photosensitizer. The photostability of compounds was investigated by recording the fluorescence emission of all IMs and INMs over 30 min while continuously irradiating at their respective excitation wavelength using the excitation and emission slit width of 14 nm. The examination of results revealed that all forms of the combination drug (IMs and INMs) were photostable for the irradiation time, as shown in Figure S11.

Light-to-Heat Conversion Efficiency.

The light-to-heat conversion efficiencies of all PTAs were investigated to determine their photothermal therapeutic potential. The increase in temperature upon irradiation of the PTA solution with light is monitored to compute the light-to-heat conversion efficiency of each compound. The results obtained for the NIR parent dyes and INMs were juxtaposed to analyze the changes in the PTT performance of the parent NIR dyes when converted to a combination ionic drug. This experiment was performed in different solvents (cell culture media, pure water, and PBS) using an 808 nm laser as an excitation source to explore the PTT behavior of the drugs in different aqueous environment. The heat efficiency graphs are shown in Figures S12–S14. Most PTAs including combination INMs exhibited an increase in temperature, indicating that sufficient heat was generated when irradiated with an 808 nm laser light source. The light-to-heat conversion efficiency was quantified using eqs S7–S10, and the results are summarized in Tables 2 and S9.

The detailed examination of the heat efficiency data revealed that all INMs' photothermal therapeutic potentials are dependent on the media. In cell culture media, all INMs showed an enhanced PTT effect as compared to their respective NIR dyes with the exception of [DOX][IR783]. Interestingly, [dOx][IR783] INM exhibited a greater heat efficiency as compared to the free NIR dye in both water and PBS, which contradicts the cell culture media results.

In contrast, [DOX][ICG] and [DOX][IR820] INMs showed lower values for light-to-heat conversion efficiency than their respective parent NIR dyes in water media (Figure S13). This could be attributed to a better cooling curve generated for the parent NIR dyes under similar experimental conditions. A decrease in the photothermal conversion efficiency for INMs as opposed to the parent NIR dye under similar experimental condition does not necessarily mean that the INM lacks PTT potential. It still possesses PTT characteristics, but it did not improve in the INM form. However, increasing the PTT efficiency of any drug requires optimization such as adjustment of the laser power and exposure timing of the PTA to irradiation. Therefore, a light-to-heat conversion efficiency experiment was conducted over a longer period (8 min) to investigate the PTT changes in [DOX][ICG] INM and ICG behavior at longer heating and cooling time range in water (Figure S13d). This led to an increased light-to-heat efficiency (33.2%) for [DOX][ICG] INM as compared to the parent NaICG dye (27.5%). However, the light absorbance behavior of NaICG did not significantly differ from the results acquired for the 5 min irradiation experiment. Moreover, a drastic change in temperature ($T_{max} - T_{sur}$) from 37.5 to 64.75 °C was observed for [DOX][ICG] INM during the 8 min experiment. This signifies the flexibility in the PTT capability of INMs upon modification of the parameters to attain the desired photothermal therapeutic effect. Even though a higher temperature change was observed for [DOX][ICG] INM at an extended time, it should be noted that a temperature greater than 49 °C has been shown to result in necrotic cell death.[10,53]

Intriguingly, an improved PTT performance was exhibited by [DOX][ICG] INMs in PBS and cell culture media compared to the free PTT NaICG dyes. Literature reported values for the specific heat capacity of PBS (1×) and cell culture media are 3.85[54] and 4.18 kJ/kg K,[55] respectively, which suggest the effect of media.

Singlet Oxygen Quantum Yield (SOQY).

There are a few reports that mentioned the PDT effect of NIR dyes.[56,57] Therefore, the ROS quantum yield experiment is designed to quantify the alterations in the ROS production of the NIR dye upon changes in the countercation. SOQY was quantified by recording the rate of decrease in absorbance of DPBF upon irradiation using an 808 nm laser. Figure S15 shows the decrease in DPBF absorbance with an increasing irradiation time in the presence of [DOX][ICG] in ethanol. A similar control experiment was designed to investigate the changes in absorbance of DPBF only after irradiation with an 808 nm laser, and the spectra at different irradiation times are shown in Figure S16. This experiment proved that DPBF absorbance only decreased under 808 nm laser irradiation in the presence of INMs. The change in absorbance of the probe was analyzed and used to compute the SOQY for all IMs and INMs, which are shown in Figures S17 and S18, respectively. In water, [DOX][IR820] and [DOX][ICG] INMs exhibited a significant increase in SOQY when compared with the free drug, as shown in Table S10. This result is very well correlated with the increased k_{nonrad}. Since intersystem crossing (ISC) is also a form of k_{nonrad}, the increased k_{nonrad} for both [DOX][IR820] and [DOX][ICG] INMs signifies a contributive effect of ISC and internal conversion (Table 1). However, [DOX][IR783] showed a decrease in SOQY, which may be ascribed to the effect of the enhanced light-to-heat conversion efficiency exhibited by the [DOX][IR783] INMs. In addition, due to the competing pathways between two non-

radiative relaxation processes, it is expected that a decrease in SOQY caused an increase in heat generation. Although the SOQY of the INMs fall within the range of 0.2–0.8% in water, [DOX][ICG] and [DOX][IR820] INMs showed improved SOQY as compared to the free parent dyes. However, the [DOX][IR783] INM did not follow the same trend. It could be attributed to the nanoformulation of the drug.

For IMs in ethanol, only [DOX][IR783] and [DOX][IR820] were found to exhibit a higher SOQY in comparison with the parent free drug (Table S10), possibly due to the higher k_{nonrad} (ISC rate) as opposed to k_{rad}. However, [DOX][ICG] SOQY in ethanol was significantly decreased, which could probably be ascribed to its increased radiative rate, decreased non-radiative rate, and high fluorescence quantum yield (Table S6). Generally, the presence of the DOX cation introduced to the PTT dye significantly altered its SOQY efficiency.

Cellular Uptake.

To prove these INMs have potential as a combination nanomedicine for cancer, several *in vitro* experiments were designed. Since the nanomedicine morphology is different from the parent soluble drugs which can impact the cellular uptake of the drug, cellular uptake experiments were performed using MCF-7 breast cancer cells. The results from the cellular uptake study of the INMs as compared to the NIR dyes after 6 h of drug incubation are shown in Figure 4. The enhanced concentration of the INMs over parent drugs in cells was quantitatively measured via a UV–visible spectrophotometer using a reported protocol.[26,58,59] Time-dependent cellular uptake experiment showed maximum uptake for both [DOX][ICG] and [DOX][IR820] in MCF-7 cells at 6 h, as depicted in Figure S19. The cellular uptake of [DOX][ICG] INMs is enhanced relative to that of NaICG parent dyes (Figure 4). In contrast, [DOX][IR783] and [DOX][IR820] only showed a slight enhancement in the cellular uptake, probably due to the morphology of nanoparticles.[26] The low cellular uptake of [DOX][IR783] is attributed to its higher PDI value.

In Vitro Cellular Toxicity of INMs.

In vitro cytotoxicity of the INMs was performed to assess the drug potency as an anticancer drug possessing dual therapeutic mechanisms (chemo and photothermal effect) when compared to the free chemotherapy or PTT drugs separately. Half-maximal inhibitory concentration (IC_{50}) values of the three INMs ([DOX][ICG], [DOX][IR820], and [DOX][IR783]) were compared to their respective parent chemo and NIR dyes (NaICG, NaIR820, and NaIR783). In the dark, the parent NIR dyes showed low cytotoxicity, as expected. The data for the dark cytotoxicity of the parent compounds and ICG containing INMs are presented in Figure 5a. Similarly, the dark cytotoxicity results for [DOX][IR820] and [DOX][IR783] INMs showed that the IC_{50} was greatly lowered as compared to those of the parent DOX and NIR dyes (Figure S20a,c). The summarized dark cytotoxicity results for all drugs are also reported in Table 3. The toxicity observed in the dark is due to the presence of DOX since the PTT mechanism of the NIR dyes can only be activated in the presence of light irradiation.[60,61] An improved DOX chemotherapeutic efficacy in the form of combination INMs revealed that DOX toxicity can be changed by tailoring the counteranion. In addition, DOX in the form of nanoparticles exhibited a lower IC_{50} in the

dark in comparison to the parent FDA-approved DOX chemotherapeutic drug due to the better cellular uptake and EPR effect of the tumor. This remarkable finding signifies the potential ability of the counterion and nanotechnology to finely tune the potency of DOX. It is possible that the toxicity of the combination drug could be further enhanced by tuning the size of nanoparticles and counterions, which is very important to inhibit the side effects of DOX. Since the combination INMs have a dual mechanism where the dark toxicity results have proven the improved toxicity of the chemotherapeutic cation in the combination INMs, light toxicity experiments are designed to investigate the photothermal effect of the anion that can only be activated in the light. Thus, the combination nanomedicines were subjected to light irradiation *in vitro*.

Photothermal Effect *In Vitro*.

To assess the potential of the INMs for use as PTAs, a light cytotoxicity experiment of the INMs was designed at 6 h using the protocol mentioned in the Experimental Section. Photothermal effect was investigated at the sixth hour due to the high cellular uptake of the INMs at that time (Figure S19). The cytotoxicity results demonstrated that the parent NIR dyes were only slightly toxic in the presence of light at a lower concentration, but increased cytotoxicity was observed at a high concentration (Figure S21). Intriguingly, the light cytotoxicity results (shown in Figures 5b and S20b,d) demonstrated that chemo-PTT combination INMs were more toxic to MCF-7 cells than the parent PTT dyes, possibly due to the higher cellular uptake, higher molar absorptivity, enhanced photothermal conversion efficiency, and higher ROS quantum yield. Since both therapeutic mechanisms (chemo and PTT) of the combination INMs will be activated in light, it is therefore crucial to examine the synergy between chemo and PTT mechanisms of the nanomedicines.

Combination Index (CI).

Degree of drug synergism is measured by the CI. In the case of a chemotherapeutic drug complexed with a photothermal therapeutic drug, the significance (additive/antagonistic/synergistic) of the effect of the chemotherapeutic drug in the presence of the photothermal drug is determined by CI.[62,63] CI is quantified by eq 2.

$$\mathrm{CI} = \frac{\mathrm{IC}_{50}(\mathrm{A}+\mathrm{B})}{\mathrm{IC}_{50}(\mathrm{A})} + \frac{\mathrm{IC}_{50}(\mathrm{A}+\mathrm{B})}{\mathrm{IC}_{50}(\mathrm{B})} \tag{2}$$

where IC_{50} (A + B) represents the IC_{50} value for the chemo-PTT combination drug and IC_{50} A or B represents the IC_{50} value of the chemotherapeutic drug and the PTT drug, respectively.

For [DOX][IR783], [DOX][IR820], and [DOX][ICG], the estimated CI values are 0.28, 0.74, and 0.32, respectively. A synergistic effect is observed for all combination nanomedicines since the CI value is lower than 1. A greater synergistic effect was observed for [DOX][IR783] INM with the lowest value of CI. NaIR783 was observed to be the least effective drug, as evident from the IC_{50} value in the light. However, when combined with

DOX, i.e., [DOX][IR783], a significantly decreased IC_{50} value was observed, which was not recorded for other INMs. This behavior resulted in a greater synergism between the chemo and the PTT drugs in [DOX][IR783] INMs.

Cell Death Mechanism.

Two experiments employing caspase 3/7 reagent and flow cytometry were designed to investigate the mechanisms of cell death. Caspase 3/7 reagent serves as a sensor for an apoptotic signal. In the presence of live cells, this reagent does not fluoresce. Caspase 3/7 DEVD peptide conjugated to DNA fluorophore cleaves whenever an apoptosis signal is detected upon drug treatment. The cleavage leads to the release of the DNA-binding fluorophore to bind to the nucleus of the apoptotic cell, generating a bright-green fluorescence emission. As observed from the confocal images in Figure 6, treatment of the cells with DOX resulted in a bright-green fluorescence. The bright-green signal observed for DOX is expected as doxorubicin is known to induce apoptosis.[64] Interestingly, the bright-green fluorescence was more prominent for the newly developed INMs, signifying an increased caspase activity. The apoptosis mechanism was further examined using flow cytometry, which offers more detailed cell death information about apoptosis and necrosis.

Flow Cytometry.

Flow cytometry enables a detailed quantitative analysis of the modes of cell death. By staining the cells with YO-PRO and PI (commercially available kits), cells undergoing both apoptosis and necrosis were analyzed.[65] When MCF-7 cells were treated with [DOX][IR783] INM for 6 h (Figure S22), the percentage of total apoptotic signal (both early and late apoptotic signals added up) slightly increased from 3.9% for DOX to about 5.2%. Necrosis effect was also observed to decrease for the newly developed INM as opposed to DOX treatment. Interestingly, during an increased drug treatment (48 h) as shown in Figure 7a–d, all INM treatments resulted in a higher percentage of apoptotic cell death. Importantly, the percentage of the total apoptotic signal increased for the three INMs as compared to soluble DOX. It was also observed that the apoptosis signal for [DOX][IR783] INM was increased 2 times as opposed to DOX with the percent apoptosis of 15.9% to about 30% for DOX and [DOX][IR783] INM, respectively. Similarly, the necrotic effect observed in all treatments was minimized for most INMs as compared to DOX. This improved cell death apoptotic mechanism could also be attributed to the effect of NIR counteranion and nanoparticle morphology. Thus, it is concluded that the DOX apoptotic cell death mechanism can be tailored using IM chemistry.

CONCLUSIONS

Three distinct combination chemo-PTT IMs were synthesized via a simple ion-exchange reaction by replacement of the chloride counterions of the chemotherapeutic drug, DOX, with three different PTT active NIR-absorbing dyes (NaICG, NaIR783, and NaIR820). By use of a simple reprecipitation method, the IMs were modified into carrier-free aqueous NPs (INMs). Improved photophysical properties were observed for NIR dyes when the sodium countercation was replaced with the DOX cation in IM and INMs. PTAs' improved molar absorptivity at longer wavelengths was only observed in combination IMs and INMs,

which makes them suitable to treat deep-seated tumors due to the deeper penetration of light. Intriguingly, all three chemo IMs and INMs also exhibit FRET capabilities. Detailed analysis of photophysical characteristics and comparison of the various radiative and non-radiative rates revealed that the INMs possessed excellent characteristics to serve as a better PTA and photosensitizer for PDT. A significant increase in the light-to-heat conversion efficiency and ROS generation upon irradiation with an 808 nm laser was also observed in combination INMs as compared to parent NIR dyes. In comparison to the routinely utilized single chemotherapeutic approach, DOX in INMs exhibited enhanced dark cytotoxicity (more than 4 times) and high cellular uptake toward MCF-7 cell lines. In addition, significantly improved light toxicity of NIR dyes was observed in INMs as compared to parent NIR dyes due to the enhanced photothermal conversion efficiency and ROS quantum yield. Moreover, combination index values of less than 1 for all INMs are indicative of the synergistic interaction of both chemo and PTT drugs used in tandem. Analysis from confocal images revealed that chemo-PTT INMs exhibited an apoptosis cell death mechanism. Increased apoptotic mechanism (almost doubled) as well as a minimal necrotic effect was observed for INMs than free chemotherapeutic drugs using flow cytometry. Collectively, these results highlight that the three INMs, [DOX][ICG], [DOX][IR820], and [DOX][IR783], are promising chemo-PTT combination drugs with great synergy. Based on the promising results generated, further studies are underway for validation prior to *in vivo*.

Supplementary Material

Refer to Web version on PubMed Central for supplementary material.

ACKNOWLEDGMENTS

This publication was made possible by the Arkansas INBRE program, supported by a grant from the National Institute of General Medical Sciences (NIGMS), P20 GM103429 from the National Institutes of Health (NIH). The authors acknowledge the financial support through the National Science Foundation Research Infrastructure under Award Number RII Track 4-1833004. Any opinions, findings, and conclusions or recommendations expressed in this material are those of the author(s) and do not necessarily reflect the views of the National Science Foundation. The authors would like to acknowledge Jeff Kamykowski and Andrea Harris at the University of Arkansas for Medical Sciences for help with TEM imaging and flow analysis, respectively. And also to appreciate the effort of Jennifer Gidden at University of Arkansas at Fayetteville, for mass spec. analysis.

REFERENCES

(1). Nierengarten MB Annual Report to the Nation on the Status of Cancer. Cancer 2023, 129 (1), 8. [PubMed: 36507862]

(2). Siegel RL; Miller KD; Wagle NS; Jemal A Cancer Statistics, 2023. CA, Cancer J. Clin 2023, 73 (1), 17–48. [PubMed: 36633525]

(3). Siegel RL; Miller KD; Fuchs HE; Jemal A Cancer Statistics, 2022. CA, Cancer J. Clin 2022, 72 (1), 7–33. [PubMed: 35020204]

(4). Yang G; Li M; Song T; Chen X; Zhang H; Wei X; Li N; Li T; Qin X; Li S; You F; Wu C; Zhang W; Liu Y; Yang H Polydopamine-Engineered Theranostic Nanoscouts Enabling Intracellular HSP90 MRNAs Fluorescence Detection for Imaging-Guided Chemo–Photothermal Therapy. Adv. Healthcare Mater 2022, 11 (23), 2201515.

(5). Wang JJ; Lei KF; Han F Tumor Microenvironment: Recent Advances in Various Cancer Treatments. Eur. Rev. Med. Pharmacol. Sci 2018, 22 (12), 3855–3864. [PubMed: 29949179]

(6). Macchi S; Zubair M; Hill R; Alwan N; Khan Y; Ali N; Guisbiers G; Berry B; Siraj N Improved Photophysical Properties of Ionic Material-Based Combination Chemo/PDT Nanomedicine. ACS Appl. Bio Mater 2021, 4 (10), 7708–7718.

(7). Rembiałkowska N; Dubińska-Magiera M; Sikora A; Szlasa W; Szewczyk A; Czapor-Irzabek H; Daczewska M; Saczko J; Kulbacka J Doxorubicin Assisted by Microsecond Electroporation Promotes Irreparable Morphological Alternations in Sensitive and Resistant Human Breast Adenocarcinoma Cells. Appl. Sci 2020, 10 (8) , 2765.

(8). Wang L; Sun Q; Wang X; Wen T; Yin JJ; Wang P; Bai R; Zhang XQ; Zhang LH; Lu AH; Chen C Using Hollow Carbon Nanospheres as a Light-Induced Free Radical Generator to Overcome Chemotherapy Resistance. J. Am. Chem. Soc 2015, 137 (5), 1947–1955. [PubMed: 25597855]

(9). Ran J; Liu T; Song C; Wei Z; Tang C; Cao Z; Zou H; Zhang X; Cai Y; Han W Rhythm Mild-Temperature Photothermal Therapy Enhancing Immunogenic Cell Death Response in Oral Squamous Cell Carcinoma. Adv. Healthcare Mater 2023, 12 (6), 2202360.

(10). Gao G; Sun X; Liang G Nanoagent-Promoted Mild-Temperature Photothermal Therapy for Cancer Treatment. Adv. Funct. Mater 2021, 31, No. 2100738, DOI: 10.1002/adfm.202100738.

(11). Du C; Wu X; He M; Zhang Y; Zhang R; Dong CM Polymeric Photothermal Agents for Cancer Therapy: Recent Progress and Clinical Potential. J. Mater. Chem. B 2021, 9 (6), 1478–1490. [PubMed: 33427844]

(12). Jiang Y; Huang C; Luan Y Lactosylated IR820/Dox Co-Assembled Nanodrug for Synergetic Antitumour Therapy. Int. J. Nanomed 2020, 15, 4431–4440.

(13). Luo T; Zhang Q; Lu Q Combination of near Infrared Light-Activated Photodynamic Therapy Mediated by Indocyanine Green with Etoposide to Treat Non-Small-Cell Lung Cancer. Cancers 2017, 9 (6), 63. [PubMed: 28587258]

(14). Starosolski Z; Bhavane R; Ghaghada KB; Vasudevan SA; Kaay A; Annapragada A Indocyanine Green Fluorescence in Second Near-Infrared (NIR-II) Window. PLoS One 2017, 12 (11), No. e0187563, DOI: 10.1371/journal.pone.0187563. [PubMed: 29121078]

(15). Tang CY; Wu FY; Yang MK; Guo YM; Lu GH; Yang YH A Classic Near-Infrared Probe Indocyanine Green for Detecting Singlet Oxygen. Int. J. Mol. Sci 2016, 17 (2), 219. [PubMed: 26861313]

(16). El-Daly SM; Gamal-Eldeen AM; Abo-Zeid MAM; Borai IH; Wafay HA; Abdel-Ghaffar ARB Photodynamic Therapeutic Activity of Indocyanine Green Entrapped in Polymeric Nanoparticles. Photodiagn. Photodyn. Ther 2013, 10 (2), 173–185.

(17). Jheng PR; Lu KY; Yu SH; Mi FL Free DOX and Chitosan-N-Arginine Conjugate Stabilized Indocyanine Green Nanoparticles for Combined Chemophotothermal Therapy. Colloids Surf., B 2015, 136, 402–412.

(18). Cui T; Li S; Chen S; Liang Y; Sun H; Wang L Stealth" Dendrimers with Encapsulation of Indocyanine Green for Photo-thermal and Photodynamic Therapy of Cancer. Int. J. Pharm 2021, 600, No. 120502. [PubMed: 33746010]

(19). Jiao L; Song F; Cui J; Peng X A Near-Infrared Heptamethine Aminocyanine Dye with a Long-Lived Excited Triplet State for Photodynamic Therapy. Chem. Commun 2018, 54 (66), 9198–9201.

(20). Thomas RG; Jeong YY NIRF Heptamethine Cyanine Dye Nanocomplexes for Multi Modal Theranosis of Tumors. Chonnam Med. J 2017, 53 (2), 83. [PubMed: 28584786]

(21). Li Y; Liu G; Ma J; Lin J; Lin H; Su G; Chen D; Ye S; Chen X; Zhu X; Hou Z Chemotherapeutic Drug-Photothermal Agent Co-Self-Assembling Nanoparticles for near-Infrared Fluorescence and Photoacoustic Dual-Modal Imaging-Guided Chemo-Photothermal Synergistic Therapy. J. Controlled Release 2017, 258, 95–107.

(22). Chen Z; Wang W; Li Y; Wei C; Zhong P; He D; Liu H; Wang P; Huang Z; Zhu W; Zhou Y; Qin L Folic Acid-Modified Erythrocyte Membrane Loading Dual Drug for Targeted and Chemo-Photothermal Synergistic Cancer Therapy. Mol. Pharmaceutics 2021, 18 (1), 386–402.

(23). Sung H; Ferlay J; Siegel RL; Laversanne M; Soerjomataram I; Jemal A; Bray F Global Cancer Statistics 2020: GLOBOCAN Estimates of Incidence and Mortality Worldwide for 36 Cancers in 185 Countries. CA, Cancer J. Clin 2021, 71 (3), 209–249. [PubMed: 33538338]

(24). Zhang A; Meng K; Liu Y; Pan Y; Qu W; Chen D; Xie S Absorption, Distribution, Metabolism, and Excretion of Nanocarriers in Vivo and Their Influences. Adv. Colloid Interface Sci 2020, 284, No. 102261.

(25). Patel V; Rajani C; Tambe V; Kalyane D; Anup N; Deb PK; Kalia K; Tekade RK Nanomaterials Assisted Chemo-Photothermal Therapy for Combating Cancer Drug Resistance. J. Drug Delivery Sci. Technol 2022, 70, No. 103164.

(26). Macchi S; Jalihal A; Hooshmand N; Zubair M; Jenkins S; Alwan N; El-Sayed M; Ali N; Griffin RJ; Siraj N Enhanced Photothermal Heating and Combination Therapy of NIR Dye via Conversion to Self-Assembled Ionic Nanomaterials. J. Mater. Chem. B 2022, 10 (5), 806–816. [PubMed: 35043823]

(27). Tang P; Liu Y; Liu Y; Meng H; Liu Z; Li K; Wu D Thermochromism-Induced Temperature Self-Regulation and Alternating Photothermal Nanohelix Clusters for Synergistic Tumor Chemo/Photothermal Therapy. Biomaterials 2019, 188, 12–23. [PubMed: 30317112]

(28). Peng L; Mei X; He J; Xu J; Zhang W; Liang R; Wei M; Evans DG; Duan X Monolayer Nanosheets with an Extremely High Drug Loading toward Controlled Delivery and Cancer Theranostics. Adv. Mater 2018, 30 (16), 1–10.

(29). Tunçel A; Yurt F Chemo-Photothermal Combination Therapy of HER-2 Overexpressing Breast Cancer Cells with Dual-Ordered Mesoporous Carbon@Silica Nanocomposite. Appl. Biochem. Biotechnol 2023, 195, 1904–1927. [PubMed: 36401724]

(30). Dreaden EC; Mwakwari SC; Sodji QH; Oyelere AK; El-Sayed MA Tamoxifen-Poly(Ethylene Glycol)-Thiol Gold Nanoparticle Conjugates: Enhanced Potency and Selective Delivery for Breast Cancer Treatment. Bioconjugate Chem. 2009, 20 (12), 2247–2253.

(31). Rennick JJ; Johnston APR; Parton RG Key Principles and Methods for Studying the Endocytosis of Biological and Nanoparticle Therapeutics. Nat. Nanotechnol 2021, 16 (3), 266–276. [PubMed: 33712737]

(32). Kus-Liśkiewicz M; Fickers P; Ben Tahar I Biocompatibility and Cytotoxicity of Gold Nanoparticles: Recent Advances in Methodologies and Regulations. Int. J. Mol. Sci 2021, 22 (20), 10952. [PubMed: 34681612]

(33). Jeyarani S; Vinita NM; Puja P; Senthamilselvi S; Devan U; Velangani AJ; Biruntha M; Pugazhendhi A; Kumar P Biomimetic Gold Nanoparticles for Its Cytotoxicity and Biocompatibility Evidenced by Fluorescence-Based Assays in Cancer (MDA-MB-231) and Non-Cancerous (HEK-293) Cells. J. Photochem. Photobiol. B 2020, 202, No. 111715.

(34). Ezealigo US; Ezealigo BN; Aisida SO; Ezema FI Iron Oxide Nanoparticles in Biological Systems: Antibacterial and Toxicology Perspective. JCIS Open 2021, 4, No. 100027.

(35). Correia DM; Fernandes LC; Fernandes MM; Hermenegildo B; Meira RM; Ribeiro C; Ribeiro S; Reguera J; Lanceros-m S Ionic Liquid-Based Materials for Biomedical Applications. Nanomaterials 2021, 11, 2401. [PubMed: 34578716]

(36). Ghandi K A Review of Ionic Liquids, Their Limits and Applications. Green Sustainable Chem. 2014, 04 (01), 44–53.

(37). Dubbelboer IR; Pavlovic N; Heindryckx F; Sjögren E; Lennernäs H Liver Cancer Cell Lines Treated with Doxorubicin under Normoxia and Hypoxia: Cell Viability and Oncologic Protein Profile. Cancers 2019, 11 (7), 1024. [PubMed: 31330834]

(38). Zeng Y; Zhan Y; Liu X; Ma J; Liu H; Li H; Yi T; Zhu Q; Du G; Zhao L; Chen D; Chen X Highly Efficient Chemo/Photothermal Therapy Alleviating Tumor Hypoxia against Cancer and Attenuate Liver Metastasis in Vivo. Chem. Eng. J 2022, 448, No. 137724.

(39). Cosco ED; Lim I; Sletten EM Photophysical Properties of Indocyanine Green in the Shortwave Infrared Region. ChemPhotoChem 2021, 5 (8), 727–734. [PubMed: 34504949]

(40). Entradas T; Waldron S; Volk M The Detection Sensitivity of Commonly Used Singlet Oxygen Probes in Aqueous Environments. J. Photochem. Photobiol. B 2020, 204, No. 111787.

(41). Shi C; Wu JB; Pan D Review on Near-Infrared Heptamethine Cyanine Dyes as Theranostic Agents for Tumor Imaging, Targeting, and Photodynamic Therapy. J. Biomed. Opt 2016, 21 (5), No. 050901.

(42). Yang X; Bai J; Qian Y The Investigation of Unique Water-Soluble Heptamethine Cyanine Dye for Use as NIR Photosensitizer in Photodynamic Therapy of Cancer Cells. Spectrochim. Acta, Part A 2020, 228, No. 117702.

(43). Reindl S; Penzkofer A; Gong SH; Landthaler M; Szeimies RM; Abels C; Bäumler W Quantum Yield of Triplet Formation for Indocyanine Green. J. Photochem. Photobiol. A 1997, 105 (1), 65–68.

(44). Giraudeau C; Moussaron A; Stallivieri A; Mordon S; Frochot C Indocyanine Green: Photosensitizer or Chromophore? Still a Debate. Curr. Med. Chem 2014, 21 (16), 1871–1897. [PubMed: 24350844]

(45). Fückel B; Roberts DA; Cheng YY; Clady RGCR; Piper RB; Ekins-Daukes NJ; Crossley MJ; Schmidt TW Singlet Oxygen Mediated Photochemical Upconversion of NIR Light. J. Phys. Chem. Lett 2011, 2 (9), 966–971.

(46). Aggarwal S; Gupta S; Gupta D; Gulzar Y; Juneja S; Alwan AA; Nauman A An Artificial Intelligence-Based Stacked Ensemble Approach for Prediction of Protein Subcellular Localization in Confocal Microscopy Images. Sustainability 2023, 15 (2), 1695.

(47). van der Velden VHJ; Preijers F; Johansson U; Westers TM; Dunlop A; Porwit A; Béné MC; Valent P; te Marvelde J; Wagner-Ballon O; Oelschlaegel U; Saft L; Kordasti S; Ireland R; Cremers E; Alhan C; Duetz C; Hobo W; Chapuis N; Fontenay M; Bettelheim P; Eidenshink-Brodersen L; Font P; Loken MR; Matarraz S; Ogata K; Orfao A; Psarra K; Subirá D; Wells DA; Della Porta MG; Burbury K; Bellos F; Weiß E; Kern W; van de Loosdrecht A Flow Cytometric Analysis of Myelodysplasia: Pre-Analytical and Technical Issues—Recommendations from the European LeukemiaNet. Cytometry, Part B 2023, 104 (1), 15–26.

(48). Danaei M; Dehghankhold M; Ataei S; Hasanzadeh Davarani F; Javanmard R; Dokhani A; Khorasani S; Mozafari MR Impact of Particle Size and Polydispersity Index on the Clinical Applications of Lipidic Nanocarrier Systems. Pharmaceutics 2018, 10 (2), 57. [PubMed: 29783687]

(49). Hoseini B; Jaafari MR; Golabpour A; Momtazi-Borojeni AA; Karimi M; Eslami S Application of Ensemble Machine Learning Approach to Assess the Factors Affecting Size and Polydispersity Index of Liposomal Nanoparticles. Sci. Rep 2023, 13 (1), No. 18012.

(50). Jalihal A; Le T; Macchi S; Krehbiel H; Bashiru M; Forson M; Siraj N Understanding of Förster Resonance Energy Transfer (FRET) in Ionic Materials. Sustainable Chem. 2021, 2 (4), 564–575.

(51). Behera SK; Mohanty ME; Mohapatra M A Fluorescence Study of the Interaction of Anticancer Drug Molecule Doxorubicin Hydrochloride in Pluronic P123 and F127 Micelles. J. Fluoresc 2021, 31 (1), 17–27. [PubMed: 33037527]

(52). Rana DK; Dhar S; Sarkar A; Bhattacharya SC Dual Intramolecular Hydrogen Bond as a Switch for Inducing Ground and Excited State Intramolecular Double Proton Transfer in Doxorubicin: An Excitation Wavelength Dependence Study. J. Phys. Chem. A 2011, 115 (33), 9169–9179. [PubMed: 21766855]

(53). Melamed JR; Edelstein RS; Day ES Elucidating the Fundamental Mechanisms of Cell Death Triggered by Photothermal Therapy. ACS Nano 2015, 9 (1), 6–11. [PubMed: 25590560]

(54). Han B; Bischof JC Thermodynamic Nonequilibrium Phase Change Behavior and Thermal Properties of Biological Solutions for Cryobiology Applications. J. Biomech. Eng 2004, 126 (2), 196–203. [PubMed: 15179849]

(55). Nikoloski N; Fröhlich J; Samaras T; Schuderer J; Küster N Reevaluation and Improved Design of the TEM Cell in Vitro Exposure Unit for Replication Studies. Bioelectromagnetics 2005, 26 (3), 215–224. [PubMed: 15768424]

(56). Lange N; Szlasa W; Saczko J; Chwiłkowska A Potential of Cyanine Derived Dyes in Photodynamic Therapy. Pharmaceutics 2021, 13 (6), 818. [PubMed: 34072719]

(57). Cao J; Chi J; Xia J; Zhang Y; Han S; Sun Y Iodinated Cyanine Dyes for Fast Near-Infrared-Guided Deep Tissue Synergistic Phototherapy. ACS Appl. Mater. Interfaces 2019, 11 (29), 25720–25729. [PubMed: 31246000]

(58). Chen M; Bhattarai N; Cong M; Pérez RL; McDonough KC; Warner IM Mitochondria Targeting IR780-Based Nano-GUMBOS for Enhanced Selective Toxicity towards Cancer Cells. RSC Adv. 2018, 8 (55), 31700–31709. [PubMed: 35548210]

(59). Forson M; Bashiru M; Macchi S; Singh S; Anderson AD; Sayyed S; Ishtiaq A; Griffin R; Ali N; Oyelere AK; Berry B; Siraj N Cationic Porphyrin-Based Ionic Nanomedicines for Improved Photodynamic Therapy. ACS Appl. Bio Mater 2023, 6 (12), 5662–5675.

(60). De U; Chun P; Choi WS; Lee BM; Kim ND; Moon HR; Jung JH; Kim HS A Novel Anthracene Derivative, MHY412, Induces Apoptosis in Doxorubicin-Resistant MCF-7/Adr Human Breast Cancer Cells through Cell Cycle Arrest and Downregulation of P-Glycoprotein Expression. Int. J. Oncol 2014, 44 (1), 167–176. [PubMed: 24190517]

(61). Pilco-Ferreto N; Calaf GM Influence of Doxorubicin on Apoptosis and Oxidative Stress in Breast Cancer Cell Lines. Int. J. Oncol 2016, 49 (2), 753–762. [PubMed: 27278553]

(62). Liu H; Zhang Z; Chi X; Zhao Z; Huang D; Jin J; Gao J Arsenite-Loaded Nanoparticles Inhibit PARP-1 to Overcome Multidrug Resistance in Hepatocellular Carcinoma Cells. Sci. Rep 2016, 6 (1), No. 31009. [PubMed: 27484730]

(63). Du C; Ding Y; Qian J; Zhang R; Dong CM Achieving Traceless Ablation of Solid Tumors without Recurrence by Mild Photothermal-Chemotherapy of Triple Stimuli-Responsive Polymer-Drug Conjugate Nanoparticles. J. Mater. Chem. B 2019, 7 (3), 415–432. [PubMed: 32254729]

(64). Kitakata H; Endo J; Ikura H; Moriyama H; Shirakawa K; Katsumata Y; Sano M Therapeutic Targets for DOX-Induced Cardiomyopathy: Role of Apoptosis vs. Ferroptosis. Int. J. Mol. Sci 2022, 23 (3), 1414. [PubMed: 35163335]

(65). Valcarce DG; Herráez MP; Chereguini O; Rodríguez C; Robles V Selection of Nonapoptotic Sperm by Magnetic-Activated Cell Sorting in Senegalese Sole (Solea Senegalensis). Theriogenology 2016, 86 (5), 1195–1202. [PubMed: 27173958]

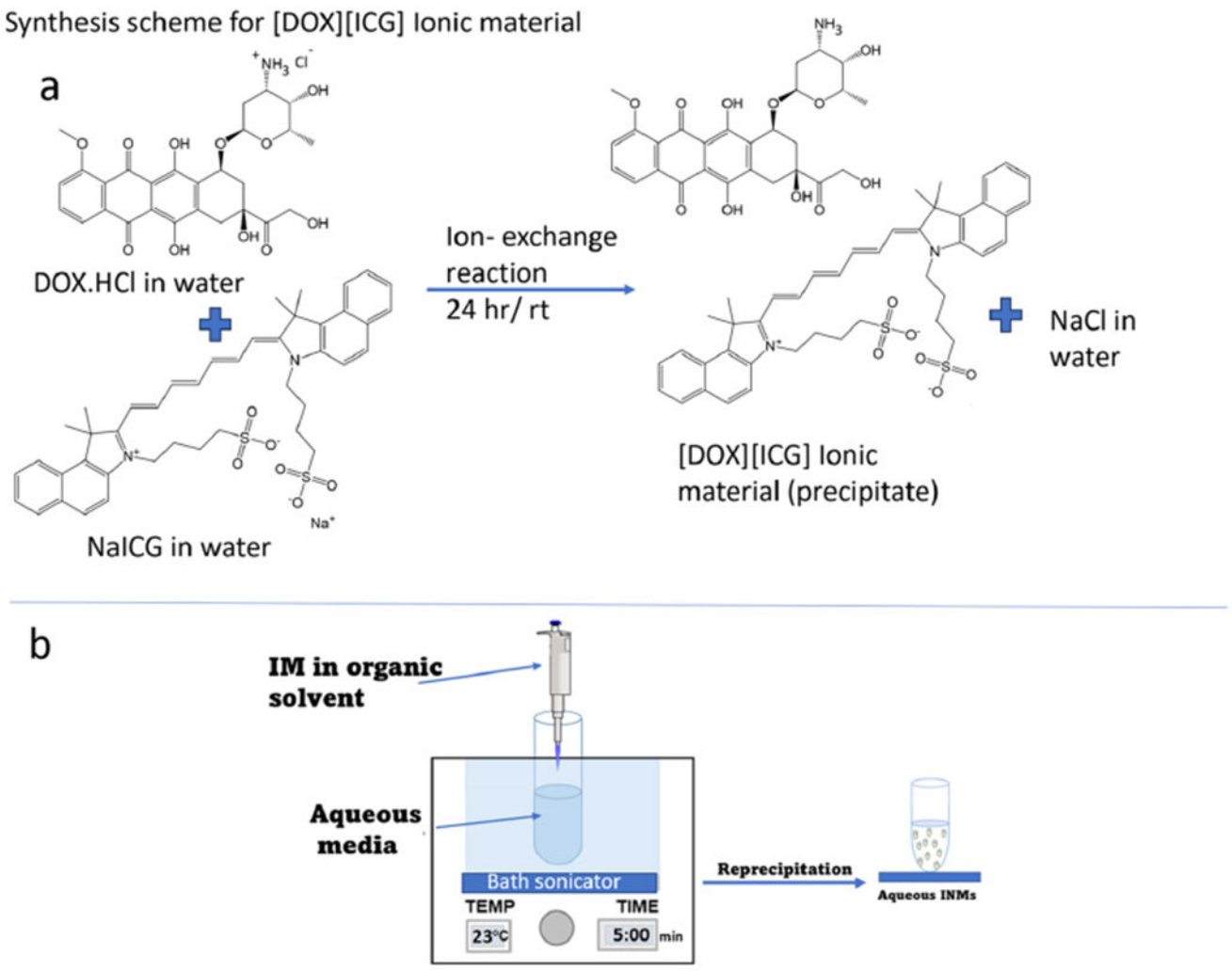

Figure 1.

(a) Synthesis of ionic material using ion-exchange reaction and (b) ionic nanomaterial synthesis.

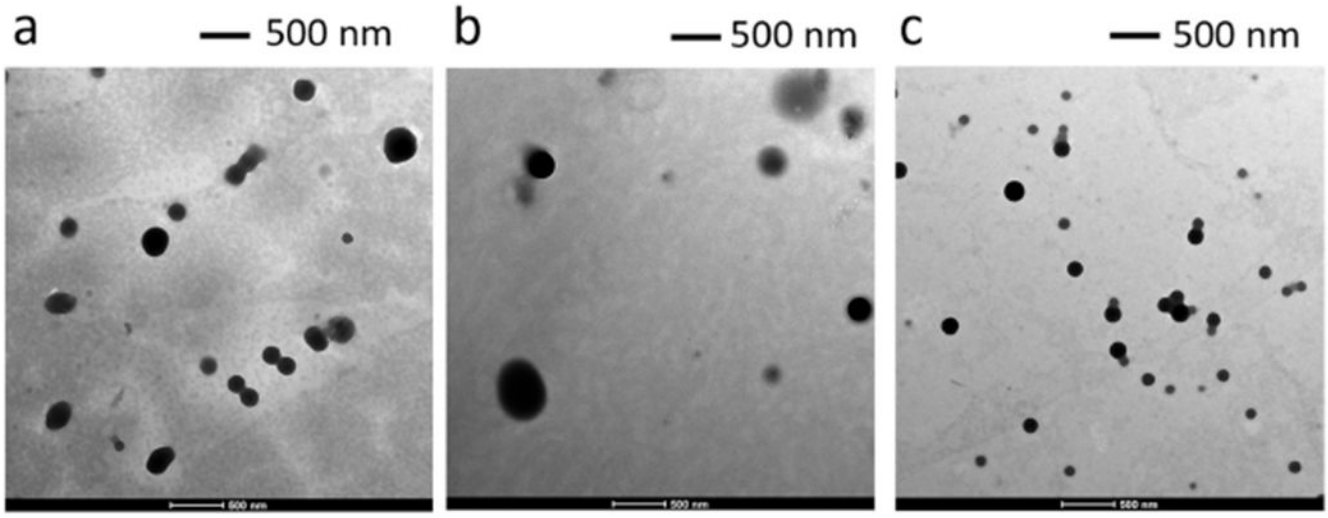

Figure 2.
TEM images for (a) [DOX][ICG], (b) [DOX][IR783], and (c) [DOX][IR820] INMs.

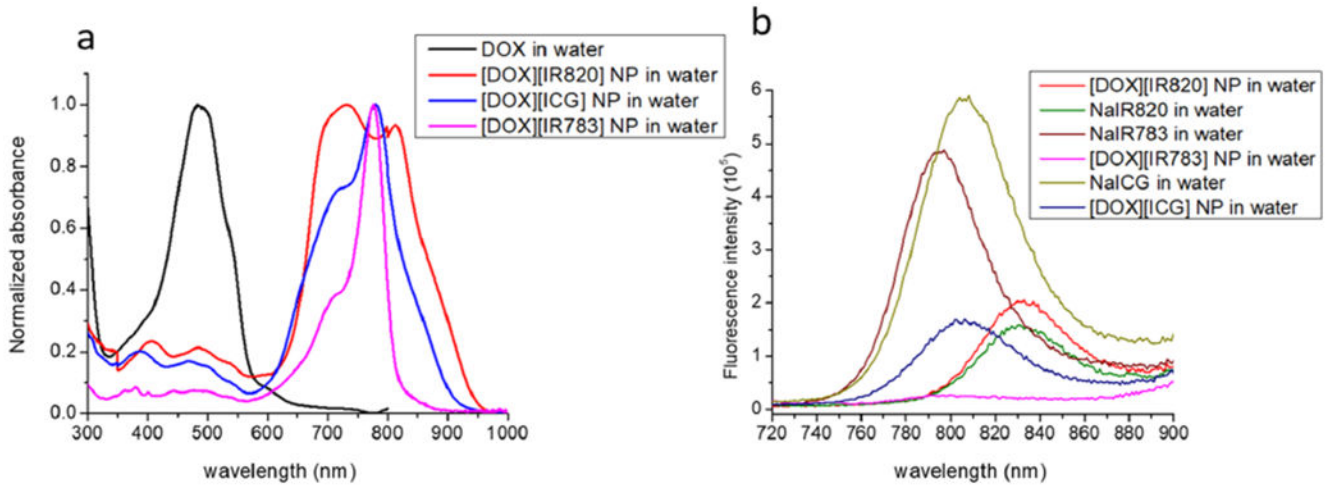

Figure 3.

(a) Normalized absorption spectra of DOX and three chemo-PTT combination INMs in water. (b) Fluorescence spectra of NIR dyes and chemo-PTT combination INMs in water at an excitation wavelength of 710 nm.

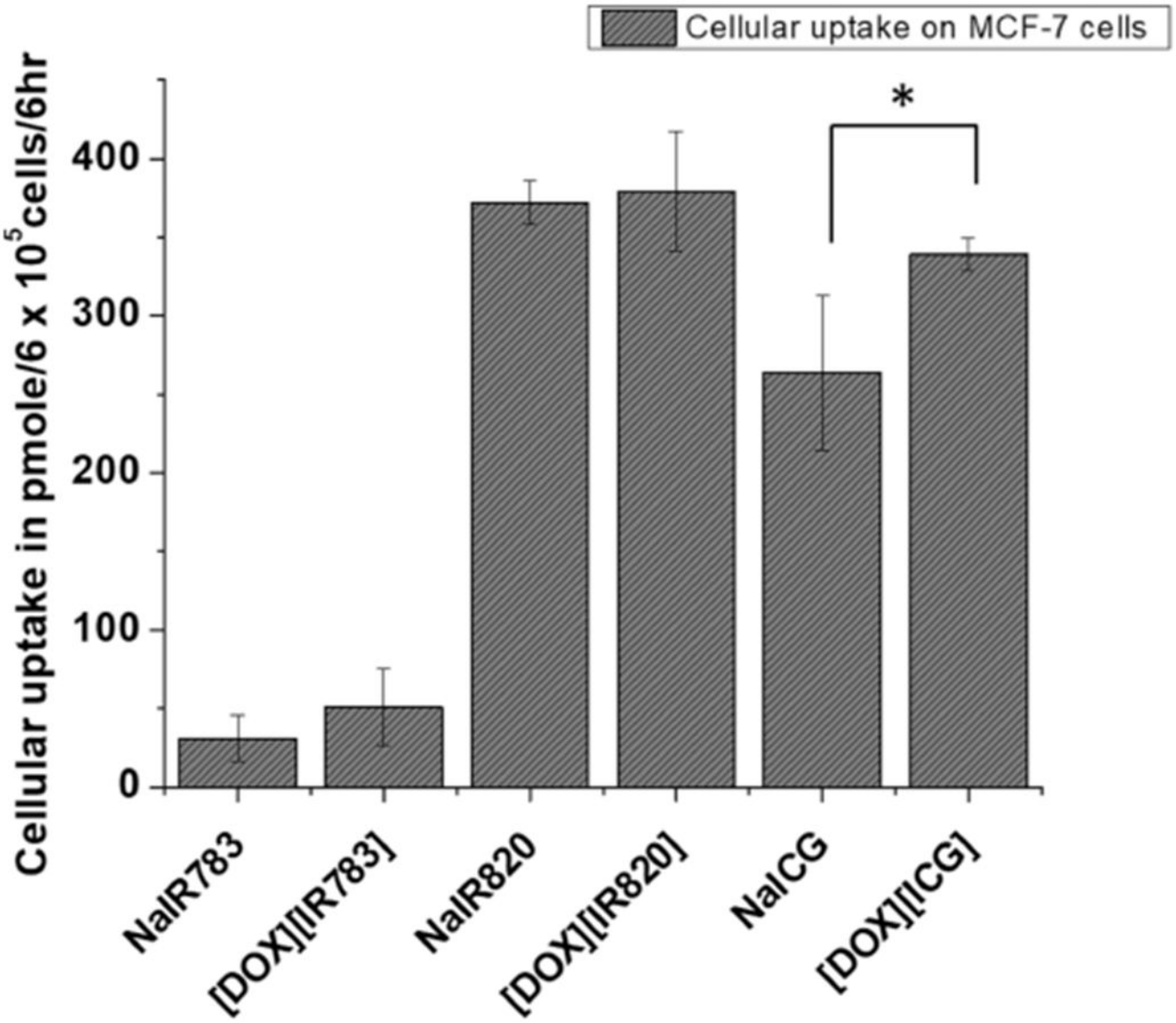

Figure 4.

Cellular uptake of three ionic nanomaterials in relation to free soluble drugs after 6 h incubation of a 60000 pmol drug in MCF-7 cancer cells. Data are presented as mean ± SD (n = 3). Data are presented as mean SD (n = 3). (*p < 0.05, **p < 0.01, ***p < 0.005).

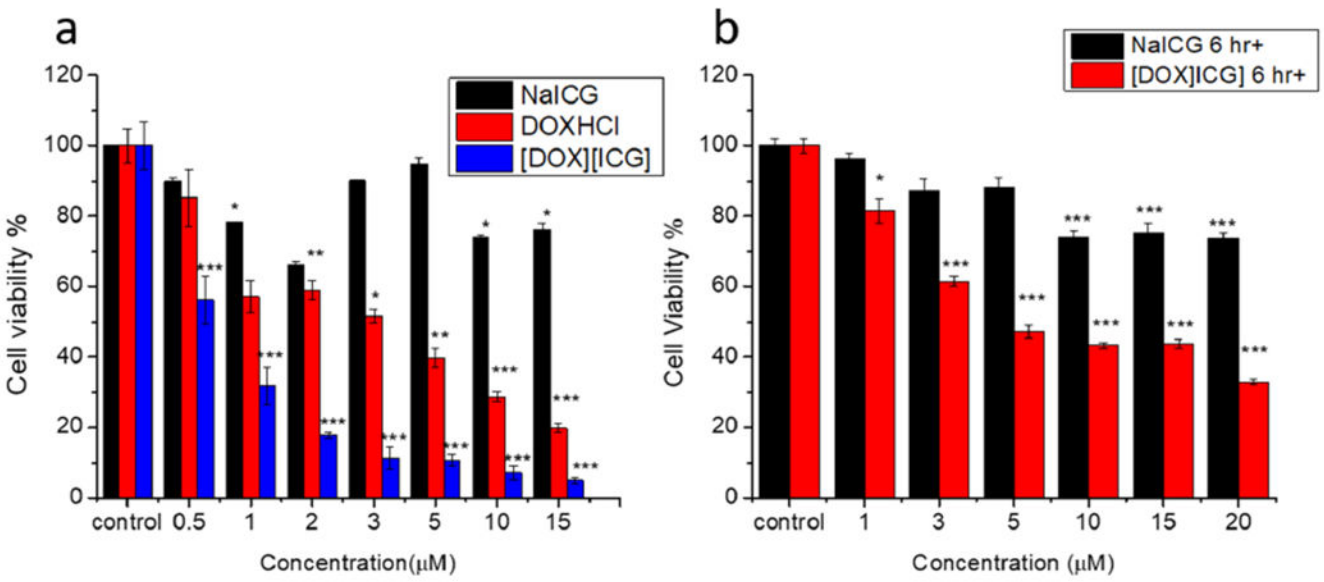

Figure 5.

(a) Cell viability results for varying concentrations of parent NaICG and doxorubicin-based drugs in MCF-7 cancer cells treated for 24 h in the dark and (b) cell viability results for NaICG and [DOX][ICG] INMs in MCF-7 cancer cells incubated for 6 h in MCF-7 cells and irradiated with 808 nm laser (1 W cm^{-2}) for 5 min. Using a two-tailed student's *t* test, p-values are determined and are presented as $*p < 0.05$, $**p < 0.01$, and $***p < 0.005$.

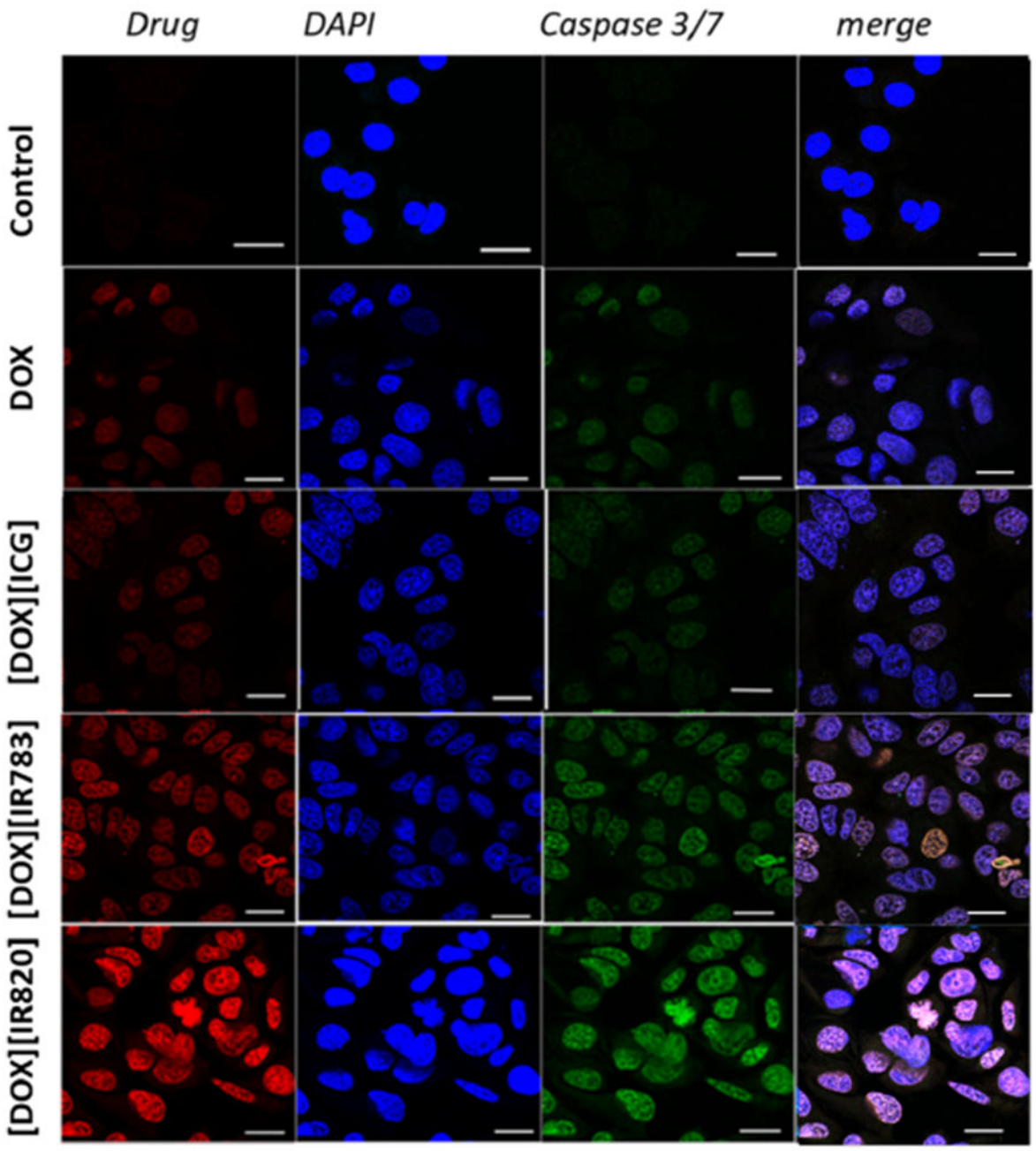

Figure 6.
Confocal microscopy imaging of caspase 3/7 activation on MCF-7 cells incubated with 5 μM DOX and three ionic nanomaterials for 6 h. Scale bar is 10 μm.

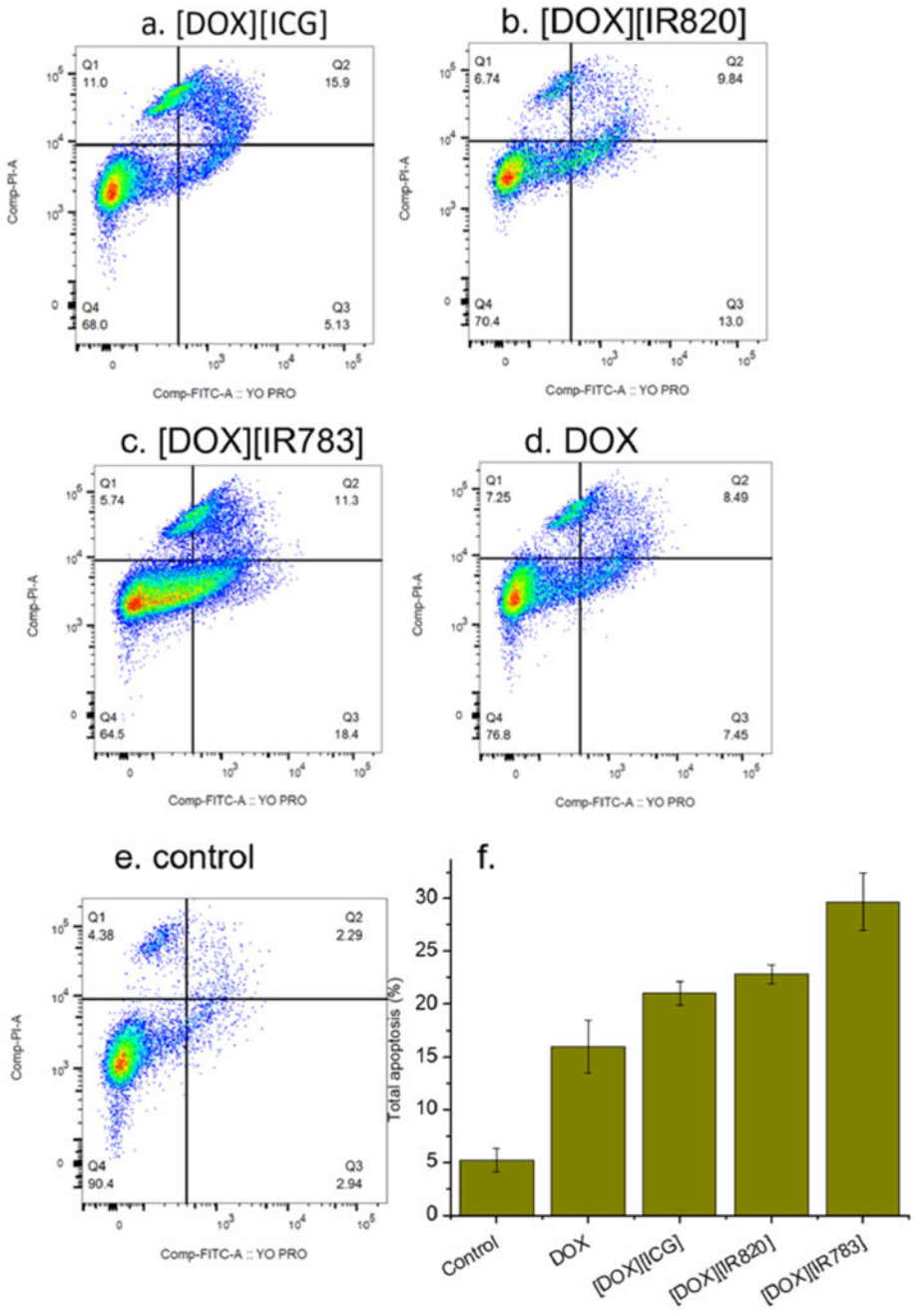

Figure 7.

(a–e) YO-PRO/propidium iodide (PI) staining results for MCF-7 cells treated with INMs and DOX after 48 h of drug incubation. Numbers in quadrants show percentages (%) of the total cell populations. (f) Data from flow cytometry experiments are represented here in the form of bar graphs. Error bars are presented as mean ± standard deviation (SD).

Table 1.

Fluorescence Quantum Yield (ϕ_F), Radiative Rate (k_{rad}), and Non-radiative Rate (k_{nonrad}) of IR Dyes and INMs in Water at 710 nm Excitation Wavelength

Drugs (INMs)	ϕ_F (%)	k_{rad} (10^7 s^{-1})	k_{nonrad} (10^7 s^{-1})
NaICG	7.1	1.9	25
[DOX][ICG]	2.6	1.9	72
NaIR820	3.4	1.2	33
[DOX][IR820]	2.5	1.7	65
NaIR783	6.7	1.7	23
[DOX][IR783]	1.0	1.6	159

Table 2.

Photothermal Efficiency for All INMs and Parent Dyes in Cell Culture Media

Compound	η, % (cell media)
NaICG	12.14
[DOX][ICG] (INMs)	26.19
NaIR820	13.51
[DOX][IR820] (INMs)	21.18
NaIR783	20.89
[DOX][IR783] (INMs)	11.50

Table 3.

Cell Viability Results for Dark and Light Study on MCF-7

Drug (INMs)	IC_{50} (dark study: 24 h)	IC_{50} (light study: 6 h+)
DOX	3.86 ± 1.03	N/A
NaICG	N/D	24.80 ± 0.72
[DOX][ICG]	0.55 ± 0.06	4.57 ± 0.57
NaIR820	N/D	24.01 ± 0.99
[DOX][IR820]	0.74 ± 0.01	11.71 ± 0.22
NaIR783	N/D	37.00 ± 1.50
[DOX][IR783]	0.89 ± 0.01	2.90 ± 0.25